1 Statistical analysis of transverse size of lower band chorus waves using 2 simultaneous multi-satellite observations 3 4 Xiao-Chen Shen¹, Wen Li¹, Qianli Ma^{2,1}, Oleksiy Agapitov³, and Yukitoshi Nishimura¹ 5 ¹ Center for Space Physics, Boston University, Boston, MA, USA. 6 ² Department of Atmospheric and Oceanic Sciences, University of California, Los Angeles, CA, 7 USA. 8 ³ Space Science Laboratory, University of California, Berkeley, CA, USA. 9 10 11 Corresponding authors: X.-C. Shen (sdusxc@gmail.com) 12 Wen Li (luckymoon761@gmail.com) 13 14 **Key Points:** 15 The average scale size of lower band chorus element is $\sim 315\pm32$ km at L shells over $\sim 5-$ 16 17 Transverse scale size of chorus is larger at higher L shells and larger at higher latitudes, 18 especially on the dayside. 19 Transverse scale size of chorus is larger in the azimuthal direction than in the radial 20 direction. 21 22

Abstract

Chorus waves are known to accelerate or scatter energetic electrons via quasi-linear or nonlinear 24 wave-particle interactions in the Earth's magnetosphere. In this letter, by taking advantage of 25 simultaneous observations of chorus waveforms from at least a pair of probes among Van Allen 26 Probes and/or Time History of Events and Macroscale Interactions during Substorms (THEMIS) 27 28 missions, we statistically calculate the transverse size of lower band chorus wave elements. The average size of lower band chorus wave element is found to be $\sim 315+32$ km over L shells of 29 ~5–6. Furthermore, our results suggest that the scale size of lower band chorus tends to be (1) 30 larger at higher L shells; (2) larger at higher magnetic latitudes, especially on the dayside; and (3) 31 larger in the azimuthal direction than in the radial direction. Our findings are crucial to quantify 32 wave-particle interaction process, particularly the nonlinear interactions between chorus and 33 energetic electrons. 34

3536

37

38

39

40

41

42

43 44

23

Plain Language Summary

Chorus waves are known to play an important role in controlling energetic electron dynamics in the Earth's magnetosphere. The spatial scale of chorus waves is one of the most important parameters that determine the wave-particle interaction process and thus is critical for understanding the role of chorus waves in radiation belt dynamics. By applying simultaneous in situ waveform observations from multiple satellites, we statistically calculate the scale size of chorus wave elements, which is found to be $\sim 315\pm32$ (95% confidence interval) km on average. More specifically, we find that the scale size tends to be larger at higher L shells, at higher magnetic latitudes, and in the azimuthal direction than in the radial direction. Our findings are crucial for understanding and modeling wave-particle interactions driven by chorus waves.

45 46

47

58

1 Introduction

- Whistler mode chorus waves are right-hand polarized electromagnetic waves with frequencies 48 below the electron cyclotron frequency (f_{ce}). They are often observed outside the plasmasphere, 49 where total electron density is relatively low and energetic electrons are injected from the plasma 50 sheet particularly during disturbed geomagnetic activities (e.g., Bell & Buneman, 1964; Katoh & 51 Omura, 2007; Omura et al., 2008; W. Li et al., 2009, 2010). An emission gap frequently exists at 52 $0.5 f_{ce}$, dividing chorus waves into lower $(0.1-0.5 f_{ce})$ and upper $(0.5-0.8 f_{ce})$ bands (e.g., Koons 53 and Roeder, 1990; Meredith et al., 2012). Chorus waves often exhibit rising and sometimes 54 falling tone features in a sub-second time scale (defined as element scale hereafter) (e.g., 55 Santolik and Gurnett, 2003; W. Li et al., 2011). Moreover, a group of chorus wave elements are 56 often clustered together and are observed on a timescale of a few seconds to 10s of seconds 57
- By accelerating or pitch angle scattering energetic electrons through quasi-linear or nonlinear interactions (e.g., Horne et al., 2003; Bortnik & Thorne, 2007; Summers et al., 2007; Bortnik et al., 2008; Tao et al., 2014; J. Li et al., 2015; Omura et al., 2015; da Silva et al., 2018), chorus waves provide a significant contribution to acceleration of highly relativistic electrons in the outer radiation belt, especially during storm times (e.g., Meredith et al., 2003; Thorne et al., 2013;

(defined as cluster scale hereafter) (W. Li et al., 2012).

- W. Li et al., 2007, 2014; Tu et al., 2014; Xiao et al., 2014; Shen et al., 2017; Bingham et al.,
- 65 2018; Ma et al., 2018; Turner et al., 2019). Moreover, chorus waves are one of the most
- important loss mechanisms of plasma sheet electrons via pitch angle scattering (e.g., Horne et al.,
- 67 2003). The scattered electrons into the upper atmosphere could then generate microbursts (e.g.,
- Nakamura et al., 2000; Breneman et al., 2017, Shumko et al., 2018), pulsating aurora (e.g.,
- 69 Nishimura et al., 2010, 2011a, 2011b; W. Li et al., 2012; Ozaki et al., 2018, 2019) and diffuse
- 70 aurora (e.g., Ni et al., 2008; Thorne et al., 2010).

In order to better understand the wave generation and wave-particle interaction processes, it is 71 crucial to know the spatial extent of chorus waves. Several studies, focusing on analyzing 72 individual events, revealed a typical scale size of chorus wave ranging from 100s to 1000s km 73 (e.g., Santolik & Gurnett, 2003; Agapitov et al., 2010, 2017). For example, Santolik and Gurnett 74 (2003) estimated the scale size of element scale chorus waves to be around 100 km by 75 calculating the correlation coefficient of wave amplitudes measured by a pair of Cluster probes at 76 $L\sim4$ on the nightside. Using Van Allen Probes (RBSP) measurements, Agapitov et al. (2017) 77 78 calculated the spatial extent of chorus elements to be 550–650 km (up to 800 km) at $L \sim 6$ on the dawnside (approximated by a Gaussian with the characteristic scale around 300 km). At a higher 79 L shell, i.e., $L \sim 11$, Agapitov et al. (2010) showed a case with a larger scale size of chorus 80 element, around 3000 km, using THEMIS observations. Moreover, the scale size of chorus 81 waves is estimated by mapping the size of microburst and pulsating aurora onto the equatorial 82 plane (e.g., Nishimura et al., 2011a, 2011b; Breneman et al., 2017; Shumko et al., 2018; Ozaki et 83 al., 2018, 2019). On the nightside at $L \sim 8$, the latitudinal (longitudinal) size of pulsating aurora 84 is found to be a few 10s (100s) kilometers, which is roughly 3000-7000 km when mapping onto 85 the equatorial plane (Nishimura et al., 2011b). Using a similar method, Ozaki et al. (2018) 86 estimated the scale size of chorus wave to be smaller, ~ 900 km at $L \sim 5$. Shumko et al. (2018) 87 showed the scale size of microburst to be ~50 km and 30 km in the latitudinal and longitudinal 88 directions respectively (from two points FIREBIRD CubeSat measurements of bouncing 89 microburst at L = 4.7) and the corresponding chorus spatial extent at the geomagnetic equator is 90 estimated to be 500-550 km. More recently, Agapitov et al. (2018) statistically analyzed the 91 scale size of chorus waves by utilizing chorus wave amplitudes from the THEMIS filter bank 92 93 data (FBK) dataset. They found that the scale size of chorus wave is largest from the dawn to noon sector, while the overall scale size is estimated to vary from 250 to 800 km, which is 94 defined as the correlation coefficient drop to 0.5. It should be noted that due to the limitation of 95 the 4-s time resolution of FBK data, the estimated scale size is more relevant to cluster scale 96 97 chorus waves.

In spite of the recent advances, many outstanding questions regarding the scale size of chorus waves still remain, especially for the chorus element scale. More specifically, (a) what is the overall scale size of chorus elements? (b) How does it vary with *L* shell, MLT and magnetic latitude (MLAT)? (c) What is the relative size of chorus wave in the radial and azimuthal direction? To address these questions, in this letter, we statistically analyze the transverse scale size of lower band chorus elements using simultaneous wave measurements from RBSP and THEMIS.

106

107

118

2 Data Set and Methodology

2.1 Instrumentation

We use measurements from the twin RBSP satellites (Mauk et al., 2013) and three of the five 108 THEMIS probes (THEMIS-A, D and E) (Angelopoulos, 2008) in this study. High time 109 resolution magnetic field measurements are from Electric and Magnetic Field Instrument Suite 110 and Integrated Science (EMFISIS) (Kletzing et al., 2013) onboard RBSP and search coil 111 magnetometer (SCM) (Le Contel et al., 2009) onboard THEMIS with the sampling frequency of 112 ~35 kHz and ~8192 Hz, respectively. These high time resolution waveform data are used to 113 calculate chorus wave properties. Background magnetic field measurements from the FluxGate 114 Magnetometers (FGM) from the two missions (Kletzing et al., 2013; Auster et al., 2008) are used 115 to calculate local electron gyrofrequency, which is then mapped to the equator using a dipole 116 field model. 117

2.2 Criterion and Calculation Method

- Conjunction criteria between a pair of probes (among RBSP and/or THEMIS missions) are set 119 as: (1) $\Delta L < 0.3$, (2) $\Delta MLT < 0.3$ h, and (3) $\Delta_{_{_{\it{I}\! I}}} < 1500$ km, where ΔL , ΔMLT , and $\Delta_{_{_{\it{I}\! I}}}$ are the 120 separation between the two probes in L shell, MLT, and the distance along the field line. 121 Moreover, both probes were required to be located between the magnetopause and the 122 plasmapause, please see the Supporting Information for more details (Meredith et al., 2004; Li et 123 al., 2014; Hartley et al., 2015), and operate the burst mode simultaneously. Note that we used the 124 criterion of Δ_{\parallel} < 1500 km, since the statistical distribution of correlation coefficients does not 125 vary significantly within ~1500 km in the parallel direction, as shown in Supporting Information 126 Figure S4. This value is consistent with the previously reported parallel scale ranging from 1200 127 to 3000 km (Santolik et al., 2004; Breneman et al., 2009; Agapitov et al., 2011). 128
- We applied the linear Pearson correlation method to calculate the correlation coefficient between the radial components (pointing away from the center of the Earth) of magnetic field waveform observed by a pair of probes in the field-aligned coordinates, where background magnetic field is calculated as the 10-minute running average. The correlation coefficient is calculated using the following equation:

$$\Gamma = \frac{\sum_{i=1}^{n} (\Psi_{x_i} - \overline{\Psi_x}) (\Psi_{y_i} - \overline{\Psi_y})}{\sqrt{\sum_{i=1}^{n} (\Psi_{x_i} - \overline{\Psi_x})^2} \sqrt{\sum_{i=1}^{n} (\Psi_{y_i} - \overline{\Psi_y})^2}} \#(1)$$

134135

136

137

where Γ is the correlation coefficient, Ψ_X is the radial component of magnetic field waveform recorded at one of the two probes (Probe X), and Ψ_Y is the radial component of magnetic field waveform recorded at the other probe (Probe Y). It is worth noting that although radial

components of wave magnetic fields are used to represent the chorus wave and calculate the

correlation coefficient, a comparison of radial and azimuthal components of wave magnetic

fields, as shown in Figure S3 of Supporting Information, indicates that the calculated correlation

coefficients are very similar.

two probes:

149

158

It is known that the background magnetic field decreases with increasing L shells in the Earth's equatorial magnetosphere. If one uses a fixed time window, one would take less wave cycles into the Γ calculation at higher L shells and hence obtain a higher correlation coefficient. Therefore, in this study, we use a varying time window based on the equatorial electron gyro frequency, specifically, 5 times of the wave cycle of $0.1 f_{ce}$ wave, to ensure that time window contains 5 (for $0.1 f_{ce}$) to 25 (for $0.5 f_{ce}$) wave cycles at various locations. A time lag τ is incorporated into the calculation considering the propagation effects and associated phase differences observed by the

$$\Gamma = \frac{\sum_{i=1}^{n} \left(\Psi_{x_i}' - \overline{\Psi_{x}'}\right) \left(\Psi_{y_i} - \overline{\Psi_{y}}\right)}{\sqrt{\sum_{i=1}^{n} \left(\Psi_{x_i}' - \overline{\Psi_{x}'}\right)^2} \sqrt{\sum_{i=1}^{n} \left(\Psi_{y_i} - \overline{\Psi_{y}}\right)^2}} \#(2)$$

where Ψ'_x is the time shifted (with time lag τ) radial component of magnetic field waveform.

Using a set of different time lags, we calculate a set of different Γ . It is worth noting that, for

periodic waves, calculated Γ would periodically change with time lag τ between -1 and 1. While

occasionally correlated signals may have a maximum value close to 1, it hardly drops close to -1.

154 Therefore, in order to remove these occasionally correlated signals, we apply:

$$\Gamma_w = \frac{Max(\Gamma) - Min(\Gamma)}{2} \#(3)$$

where $Max(\Gamma)$ is the maximum Γ with a set of time lags, while $Min(\Gamma)$ is the minimum. In this

way, the calculated Γ_w for periodic waves almost stays the same, however, Γ significantly

deceases for occasionally correlated signals.

2.3 Case study on 22 Jan 2016

Figure 1 shows an example of simultaneous observations of chorus waves from RBSP-A and B.

On 22 Jan 2016, RBSP-A and B were closely located with the separation distances of 226, 183,

and 447 km in the radial, azimuthal and parallel direction relative to the ambient field line,

respectively. Both probes observed strong lower band rising tone chorus emissions, as shown in

Figures 1a, 1b, 1h and 1i. Many weak chorus emissions exhibit slightly oblique wave normal

angles, while large amplitude emissions are very parallel to the background magnetic field line

165 (Figures 1c, 1d, 1j and 1k).

Figure 1e shows Γ as a function of universal time (UT) and time lag. The time lag shown here is

limited to ± 2 ms to visualize the periodic structures at each time slice more clearly. However, the

actual time lag considered in calculating Γ could be up to 0.1 s. It is evident that with different

time lags, correlation coefficient shows periodic changes, which is clearer in a zoom-in view

shown in Figure 11. Γ_w calculated from Equation (3) is shown in Figure 1g. In this study, we

focus on lower band chorus emissions which exhibit rising or falling tone features with magnetic

wave amplitudes $(B_{\rm w})$ over 0.1–0.5 $f_{\rm ce}$ well above the noise level. Therefore, we select $\Gamma_{\rm w}$ with

 $B_{\rm w}$ greater than the larger value between 5 pT and 2 times of the median of $B_{\rm w}$ in the 6-sec time

window from 07:47:00 UT to 07:47:06 UT (marked with black dots in Figures 1g and 1n). It is

worth noting that weak chorus elements have similar wave amplitudes to the hiss-like waves

around 1 kHz, thus are not included in calculating correlation coefficients by applying the $B_{\rm w}$

177 criterion.

187

188

During this time interval, the median, upper quartile (75th percentile) and maximum of the 178 selected $\Gamma_{\rm w}$ are 0.56, 0.66 and 0.86, respectively. We select the 75th percentile, i.e., 0.66, to 179 represent the correlation coefficient for this conjunction event. The reason why we use a 180 relatively large percentile is that even when the satellite separation is smaller than the chorus 181 scale size, one of the probes may possibly be located outside the chorus region leading to a low 182 correlation coefficient, which is likely more obvious when the satellite separation is comparable 183 to the chorus scale size. Nevertheless, the calculated statistical scale size of chorus wave 184 elements using median values (see section 3 below) is similar to that using 75th percentile values, 185 indicating that our calculation is robust. 186

3 Statistical Results

3.1 Overall Transverse Scale Size

- After applying all the criteria described above, we identified more than two thousand conjugate
- events during five years from January 2013 to December 2017. Figures 2a and 2b show
- distributions of these events in the L-MLT and L-MLAT planes. The majority of events are
- collected from the twin RBSP conjunctions, which are mostly distributed at L shells between 5
- and 6. On the duskside, only a few conjugate events are observed, which is reasonable since the
- dusk-side magnetosphere is not favorable for chorus generation (Meredith et al., 2003, 2012; W.
- 195 Li et al., 2010).
- 196 Figures 2c and 2d show the number of events and correlation coefficients as a function of
- transverse separation distance (Δ_{\perp}), which is calculated in the field-aligned coordinate system.
- 198 Here, the field-aligned coordinate is defined based on a 15-min running average of the
- background magnetic field observed by RBSP-A or RBSP-B, depending on which one of the two
- 200 probes is located closer to the equator during the event. As shown in Figure 2d, the calculated
- correlation coefficient tends to decease with increasing Δ_{\perp} . The dark blue line is a Gaussian
- fitting for the averaged correlation coefficient within each Δ_{\perp}^{-} bin (magenta dots):

$$f(x) = A_0 e^{-\frac{x^2}{2A_1^2}} + A_2 \#(4)$$

- where $(A_0 + A_2)$ is the peak of the Gaussian distribution and A_1 is the half width of the fitting.
- 204 Center of the fitting is set to be zero, where the separation is the smallest and the correlation
- coefficient is expected be the largest. The peak and half width of the Gaussian fitting are around
- 206 0.68 and 315 ± 32 (95% confidence interval) km, respectively. The peak is below 1 which may
- be due to the parallel separation. The overall scale size of chorus elements is $\sim 315\pm32$ km,

which is defined as the half width of the Gaussian fitting, and is up to 450 km where the correlation coefficient drops to 0.5. It should be noted that if we use median values of correlation coefficients (rather than 75th percentiles) in each 6-s time window, the scale size of chorus wave is ~306 km, which is slightly smaller but is very close to the value using 75th percentiles, indicating the robustness of our calculation.

3.2 L, MLT and MLAT Dependence

213

244

The dependences of chorus wave scale size on L shell, MLT and MLAT are further evaluated 214 and shown in Figure 3. Figure 3a shows the averaged correlation coefficient sorted by various L 215 and MLT bins. Note that only events with $\Delta_1 \leq 800$ km are included, which is roughly the 216 transverse size when the fitted correlation coefficient drops to 0.4 in Figure 2d, to reduce the 217 transverse separation influence. It is also worth noting that we did not use the half width value 218 (315 km) as the threshold value due to the limited event samples within that transverse 219 separation. Bins with the number of events less than ten are excluded on the top row in Figure 3 220 due to the relatively low statistical significance. Average correlation coefficients are relatively 221 larger over 6-12 MLT, compared to other MLT bins. Interestingly, average correlation 222 coefficient tends to be larger at higher L shells for all the four MLT bins, which suggests a trend 223 that chorus scale size tends to increase at higher L shells. This feature is reasonable, since the 224 magnetic field intensity decreases with increasing L shells, leading to increasing Larmor radius 225 of source electrons, which may be relevant to increasing transverse scale size of chorus waves. It 226 is worthwhile to note that the correlation coefficient shown in the bottom-left (5.5–5.6 L shell 227 and 0-6 MLT) and top-right bins (5.8-5.9 L shell and 18-24 MLT) of Figure 3a may not be 228 statistically significant since the top-right (bottom-left) bin has a few conjugate events whose 229 transverse separations are small (large), respectively. 230

Figures 3c and 3d (Figures 3e and 3f) show the binned correlation coefficient and number of 231 events in each MLT- Δ_{\perp} bin for magnetic latitude within 7 degrees (larger than 7 degrees). The 232 average correlation coefficient tends to decrease with increasing transverse separation distance in 233 both $|MLAT| < 7^{\circ}$ (Figure 3c) and $|MLAT| > 7^{\circ}$ (Figure 3e). Interestingly, averaged correlation 234 coefficients are typically larger at higher latitudes (|MLAT| > 7°) than those at lower latitudes 235 (|MLAT| < 7°), especially closer to the noon. A possible mechanism for the MLAT dependence 236 of chorus scale size could be the geometrical spreading of wave power, since the waves tend to 237 become more oblique and thus deviate from the original L shell during their propagation from 238 the equator towards higher latitudes, as revealed from ray tracing simulations (e.g., Breuillard et 239 al., 2013; Chen et al., 2013). This effect is more distinct closer to the dayside, indicating that a 240 compressed magnetic field topology (e.g., Keika et al., 2012) may be more favorable for the 241 wave power spreading than a stretched field line at least within ~20° of magnetic latitude where 242 RBSP/THEMS wave measurements are available. 243

3.3 Azimuthal Versus Radial Size

Furthermore, we divide the transverse separation into the azimuthal and radial directions to compare the scale size of lower band chorus elements in these two directions. Figures 4a and 4b

show averaged correlation coefficient and number of events in each $\Delta r \times \Delta \varphi$ bin, where Δr is the radial separation and $\Delta \varphi$ is the azimuthal separation. Bins with fewer than ten event samples are not shown. Due to the fact that the burst mode operates more frequently when the dual Van Allen Probes are getting closer, more event samples are obtained at smaller separations. From Figure 4a, as expected, a larger correlation coefficient is found for a smaller separation in both directions. More interestingly, the binned correlation coefficient decreases faster in the azimuthal direction than in the radial direction within ~600 km. However, it remains above 0.4 within ~1000 km in the azimuthal direction, which is larger than that in the radial direction. This finding suggests that chorus waves may remain phase coherent in a larger spatial extent along the azimuthal direction, which may be caused by the azimuthal drift motion of source electrons after their injection from the plasma sheet. It is also important to note that, in the azimuthal direction, the correlation coefficient does not show smooth variations which may also be influenced by the drift motion of source particles, whose drift speed depends on energy.

4 Summary and Discussion

- We use simultaneous multi-probe observations (i.e., at least a pair of probes from Van Allen Probes and/or THEMIS missions) of chorus waveforms to calculate the transverse scale size of lower band chorus waves in the element scale. Main findings are summarized as follows.
 - 1. Overall, at L shells over 5–6 an average transverse scale size of lower band chorus wave, calculated based on the half width of Gaussian fitting of correlation coefficients, is about 315 ± 32 km and is up to 450 km where the correlation coefficient drops to 0.5.
 - 2. Averaged correlation coefficient tends to become larger at higher *L* shells at all MLT bins (Figure 3a), suggesting that transverse scale size of lower band chorus wave tends to be larger at higher *L* shells.
 - 3. Averaged correlation coefficient is larger at higher latitudes (Figures 3c and 3e), suggesting that the scale size tends to become larger at higher latitudes. This feature is more significant on the dayside, where the magnetic field is more compressed.
 - 4. The scale size of chorus waves is slightly larger in the azimuthal direction than in radial direction, which may be caused by the drift motion of source electrons in the azimuthal direction.

Interestingly, from THEMIS FBK statistics, Agapitov et al. (2018) found that cluster scale chorus waves with larger $B_{\rm w}$ have smaller scale sizes, which may be consistent with our results, since larger $B_{\rm w}$ chorus waves are more likely observed near the equator region, especially in the nightside magnetosphere (W. Li et al., 2009). Moreover, the scale size of cluster scale chorus waves is larger on the dayside than on the nightside, which is suggested to be caused by the fact that injected energetic electrons spread wider as they drift from the nightside to the dayside (Agapitov et al., 2018). Thus, it is not surprising that a relatively small scale size of chorus waves, ~100 km, was reported by Santolik et al. (2003) near 21 MLT. This effect may also contribute to the MLT dependence of element scale size of chorus waves in our statistical study that the scale size becomes larger away from the nightside where energetic electrons are closer to the initial injection region. The number of samples is small on the duskside, thus the result that

- the scale size decreases after 12 MLT needs further validations in future studies.
- It is worth noting that since most conjunction events were collected by the dual RBSP satellites
- near their apogee (L shells between 5 and 6), although we use THEMIS and RBSP satellite
- 290 constellations, the scale size may be more representative for the lower band chorus waves over
- 291 the L shells of 5–6. Nevertheless, the extensive waveform data set in this region provided an
- excellent opportunity to statistically evaluate the dependence of chorus scale size on L shell,
- MLT, and magnetic latitudes. The L shell dependence covering a broader range of L shells is
- beyond the scope of the present study, and is left for future investigations.

296

312313

Acknowledgments

- 297 XS and WL would like to acknowledge the NSF grant AGS-1847818, the NASA grants
- 298 NNX17AG07G, 80NSSC19K0845, the AFOSR grant FA9550-15-1-0158, and the Alfred P.
- Sloan Research Fellowship FG-2018-10936. The work of OA was supported by the NASA Grant
- NNX16AF85G, THEMIS NASA contract NAS5-02099, and JHU/APL contract 922613 (RBSP-
- EFW). The work of YN was supported by the NASA grant 80NSSC18K0657 and NSF grant
- PLR-1341359. We acknowledge the Van Allen Probes mission, particularly the EMFISIS team
- for providing the wave data. We acknowledge NASA contract NAS5-02099 and V.
- Angelopoulos for use of data from the THEMIS Mission. Specifically: O. LeContel and the late
- A. Roux for use of SCM data, and K. H. Glassmeier, U. Auster and W. Baumjohann for the use
- of FGM data provided under the lead of the Technical University of Braunschweig and with
- financial support through the German Ministry for Economy and Technology and the German
- Center for Aviation and Space (DLR) under contract 50 OC 0302.
- Van Allen Probes FGM and EMFISIS data are obtained from the website:
- 310 https://emfisis.physics.uiowa.edu/Flight/. THEMIS FGM and SCM data are obtained from the
- website: http://themis.ssl.berkeley.edu/data/themis/.

References

- Agapitov, O., Blum, L. W., Mozer, F. S., Bonnell, J. W., & Wygant, J. (2017). Chorus whistler
- wave source scales as determined from multipoint Van Allen Probe measurements. Geophysical
- Research Letters, 44(6), 2634–2642.
- Agapitov, O., Krasnoselskikh, V., Zaliznyak, Y., Angelopoulos, V., Le Contel, O., & Rolland,
- G. (2010). Chorus source region localization in the Earth's outer magnetosphere using THEMIS
- measurements. Annales Geophysicae, 28(6), 1377–1386.
- Agapitov, O., Krasnoselskikh, V., Dudok de Wit, T., Khotyaintsev, Y., Pickett, J. S., Santolík, O.,
- & Rolland, G. (2011). Multispacecraft observations of chorus emissions as a tool for the plasma
- density fluctuations' remote sensing. Journal of Geophysical Research: Space Physics (1978–
- 324 2012), 116(A9).
- Agapitov, O., Mourenas, D., Artemyev, A., Mozer, F. S., Bonnell, J. W., Angelopoulos, V., . . .
- Krasnoselskikh, V. (2018). Spatial Extent and Temporal Correlation of Chorus and Hiss:
- 327 Statistical Results from Multipoint THEMIS Observations. Journal of Geophysical Research:
- 328 Space Physics, 123 (10), 8317–8330.
- Angelopoulos, V. (2008), The THEMIS Mission, Space Sci. Rev., 141 (1-4), 5-34,
- 330 doi:10.1007/s11214-008-9336-1.
- Auster, H. U., Glassmeier, K. H., Magnes, W., Aydogar, O., Baumjohann, W., Constantinescu,
- D., ... Wiedemann, M. (2008). The THEMIS Fluxgate Magnetometer. Space Science Reviews,
- 333 141(1-4), 235–264.
- Bell, T. F., & Buneman, O. (1964). Plasma Instability in the Whistler Mode Caused by a
- Gyrating Electron Stream. Physical Review, 133(5A), A1300–A1302.
- Bingham, S. T., Mouikis, C. G., Kistler, L. M., Boyd, A. J., Paulson, K., Farrugia, C. J., ...
- Kletzing, C. (2018). The Outer Radiation Belt Response to the Storm Time Development of Seed
- Electrons and Chorus Wave Activity During CME and CIR Driven Storms. Journal of
- 339 Geophysical Research: Space Physics, 123(12), 10,139–10,157.
- Bortnik, J., & Thorne, R. M. (2007). The dual role of ELF/VLF chorus waves in the acceleration
- and precipitation of radiation belt electrons. Journal of Atmospheric and Solar-Terrestrial
- 342 Physics, 69(3), 378–386.
- Bortnik, J., Thorne, R. M., & Inan, U. S. (2008). Nonlinear interaction of energetic electrons
- with large amplitude chorus. Geophysical Research Letters, 35(2), L21102.
- Breneman, A. W., Kletzing, C. A., Pickett, J., Chum, J., & Santolik, O. (2009). Statistics of
- multispacecraft observations of chorus dispersion and source location. Journal of Geophysical
- 347 Research: Space Physics, 114(A6), A06202.

- Breneman, A. W., Crew, A., Sample, J., Klumpar, D., Johnson, A., Agapitov, O., ... Kletzing,
- 349 C. A. (2017). Observations Directly Linking Relativistic Electron Microbursts to Whistler Mode
- Chorus: Van Allen Probes and FIREBIRD II. Geophysical Research Letters, 44(22), 11,265–
- 351 11,272.
- Breuillard, H., Zaliznyak, Y., Agapitov, O., Artemyev, A., Krasnoselskikh, V., & Rolland, G.
- 353 (2013). Spatial spreading of magnetospherically reflected chorus elements in the inner
- 354 magnetosphere. Ann. Geophys., 31(8), 1429–1435.
- Chen, L., R. M., Thorne, W., Li, and J., Bortnik (2013), Modeling the wave normal distribution
- of chorus waves, J. Geophys. Res. Space Physics, 118, 1074–1088.
- Hartley, D. P., Y. Chen, C. A. Kletzing, M. H. Denton, and W. S. Kurth (2015), Applying the
- cold plasma dispersion relation to whistler mode chorus waves: EMFISIS wave measurements
- 359 from the Van Allen Probes, J. Geophys. Res. Sp. Phys., 120(2), 1144–1152,
- 360 doi:10.1002/2014JA020808.
- Horne, R. B., Glauert, S. A., & Thorne, R. M. (2003). Resonant diffusion of radiation belt
- electrons by whistler-mode chorus. Geophysical Research Letters, 30(9), 1493.
- Katoh, Y., & Omura, Y. (2007). Computer simulation of chorus wave generation in the Earth's
- inner magnetosphere. Geophysical Research Letters, 34(3), 235.
- Keika, K., M. Spasojevic, W. Li, J. Bortnik, Y. Miyoshi, and V. Angelopoulos (2012),
- PENGUIn/AGO and THEMIS conjugate observations of whistler mode chorus waves in the
- dayside uniform zone under steady solar wind and quiet geomagnetic conditions, J. Geophys.
- 368 Res., 117, A07212, doi:10.1029/2012JA017708.
- Kletzing, C. A., Kurth, W. S., Acuna, M., MacDowall, R. J., Torbert, R. B., Averkamp, T., . . .
- 370 Tyler, J. (2013). The Electric and Magnetic Field Instrument Suite and Integrated Science
- 371 (EMFISIS) on RBSP. Space Science Reviews, 179(1-4), 127–181.
- Koons, H. C., and J. L. Roeder (1990), A survey of equatorial magnetospheric wave activity
- between 5 and 8 RE, Planet. Space Sci., 38(10), 1335–1341, doi:10.1016/0032-0633(90)90136-
- 374 E
- Le Contel, O., Roux, A., Robert, P., Coillot, C., Bouabdellah, A., de la Porte, B., . . . Larson, D.
- (2009). First Results of the THEMIS Search Coil Magnetometers. In The themis mission (pp.
- 509–534). New York, NY: Springer, New York, NY.
- Li, J., Bortnik, J., Xie, L., Pu, Z., Chen, L., Ni, B., . . . Guo, R. (2015). Comparison of formulas
- for resonant interactions between energetic electrons and oblique whistler-mode waves. Physics
- of Plasmas, 22(5), 052902. doi: 10.1063/1.4914852
- Li, W., Shprits, Y. Y., & Thorne, R. M. (2007). Dynamic evolution of energetic outer zone

- electrons due to wave-particle interactions during storms. Journal of Geophysical Research:
- 383 Space Physics, 112(A), A10220.
- Li, W., Thorne, R. M., Angelopoulos, V., Bonnell, J. W., McFadden, J. P., Carlson, C. W., . . .
- Auster, H. U. (2009). Evaluation of whistler-mode chorus intensification on the nightside during
- an injection event observed on the THEMIS spacecraft. Journal of Geophysical Research,
- 387 114(8), A00C14.
- Li, W., Thorne, R. M., Nishimura, Y., Bortnik, J., Angelopoulos, V., McFadden, J. P., ...
- Auster, U. (2010). THEMIS analysis of observed equatorial electron distributions responsible for
- the chorus excitation. Journal of Geophysical Research, 115(1), A00F11.
- Li, W., Thorne, R. M., Bortnik, J., Shprits, Y. Y., Nishimura, Y., Angelopoulos, V., ... Bonnell,
- J. W. (2011). Typical properties of rising and falling tone chorus waves. Geophysical Research
- 393 Letters, 38(1), L14103.
- Li, W., Bortnik, J., Nishimura, Y., Thorne, R. M., & Angelopoulos, V. (2012). The Origin of
- Pulsating Aurora: Modulated Whistler Mode Chorus Waves. Auroral Phenomenology and
- Magnetospheric Processes: Earth and Other Planets, 197.
- Li, W. et al. (2014), Evidence of stronger pitch angle scattering loss caused by oblique whistler-
- mode waves as compared with quasi-parallel waves, Geophys. Res. Lett., 41(17), 6063–6070,
- 399 doi:10.1002/2014GL061260.
- 400 Li, W., Thorne, R. M., Ma, Q., Ni, B., Bortnik, J., Baker, D. N., . . . Claudepierre, S. G. (2014).
- Radiation belt electron acceleration by chorus waves during the 17 March 2013 storm. Journal of
- Geophysical Research: Space Physics, 119(6), 4681–4693.
- 403 Ma, Q., Li, W., Bortnik, J., Thorne, R. M., Chu, X., Ozeke, L. G., ... Claudepierre, S. G. (2018).
- 404 Quantitative Evaluation of Radial Diffusion and Local Acceleration Processes During GEM
- Challenge Events. Journal of Geophysical Research: Space Physics, 123(3), 1938–1952.
- Mauk, B., N. J. Fox, S. Kanekal, R. Kessel, D. Sibeck, and A. Ukhorskiy (2013), Science
- objectives and rationale for the radiation belt storm probes mission, Space Sci. Rev., 179, 3–27.
- Meredith, N. P., Horne, R. B., Thorne, R. M., & Anderson, R. R. (2003). Favored regions for
- 409 chorus-driven electron acceleration to relativistic energies in the Earth's outer radiation belt.
- Geophysical Research Letters, 30(1), 1871.
- Meredith, N. P., Horne, R. B., Thorne, R. M., Summers, D., and Anderson, R. R. (2004),
- Substorm dependence of plasmaspheric hiss, J. Geophys. Res., 109, A06209,
- 413 doi:10.1029/2004JA010387.
- Meredith, N. P., Horne, R. B., Sicard-Piet, A., Boscher, D., Yearby, K. H., Li, W., & Thorne, R.
- 415 M. (2012). Global model of lower band and upper band chorus from multiple satellite

- observations. Journal of Geophysical Research, 117(A), A10225.
- Nakamura, R., Isowa, M., Kamide, Y., Baker, D. N., Blake, J. B., & Looper, M. (2000).
- SAMPEX observations of precipitation bursts in the outer radiation belt. Journal of Geophysical
- 419 Research: Space Physics, 105(A7), 15875–15885.
- Ni, B., Thorne, R. M., Shprits, Y. Y., & Bortnik, J. (2008). Resonant scattering of plasma sheet
- electrons by whistler-mode chorus: Contribution to diffuse auroral precipitation. Geophysical
- 422 Research Letters, 35(11), 135.
- Nishimura, Y., Bortnik, J., Li, W., Thorne, R. M., Lyons, L. R., Angelopoulos, V., ... Auster,
- 424 U. (2010). Identifying the Driver of Pulsating Aurora. Science, 330(6000), 81–84.
- Nishimura, Y., Bortnik, J., Li, W., Thorne, R. M., Lyons, L. R., Angelopoulos, V., ... Auster,
- 426 U. (2011a). Estimation of magnetic field mapping accuracy using the pulsating aurora-chorus
- connection. Geophysical Research Letters, 38(1), L14110.
- Nishimura, Y., Bortnik, J., Li, W., Thorne, R. M., Chen, L., Lyons, L. R., ... Auster, U. (2011b).
- 429 Multievent study of the correlation between pulsating aurora and whistler mode chorus
- emissions. Journal of Geophysical Research, 116(A), A11221.
- Omura, Y., Katoh, Y., & Summers, D. (2008). Theory and simulation of the generation of
- whistler-mode chorus. Journal of Geophysical Research: Space Physics, 113(A), A04223.
- Omura, Y., Miyashita, Y., Yoshikawa, M., Summers, D., Hikishima, M., Ebihara, Y.,
- and Kubota, Y. (2015), Formation process of relativistic electron flux through interaction with
- chorus emissions in the Earth's inner magnetosphere, J. Geophys. Res. Space Physics, 120,9545–
- 436 9562.
- Ozaki, M., Miyoshi, Y., Shiokawa, K., Hosokawa, K., Oyama, S.-i., Kataoka, R., . . . Shinohara,
- 438 I. (2019). Visualization of rapid electron precipitation via chorus element wave–particle
- interactions. Nature Communications, 10(1), 257.
- Ozaki, M., Shiokawa, K., Miyoshi, Y., Hosokawa, K., Oyama, S., Yagitani, S., . . . Shinohara, I.
- 441 (2018). Microscopic Observations of Pulsating Aurora Associated with Chorus Element
- Structures: Coordinated Arase Satellite-PWING Observations. Geophysical Research Letters,
- 443 45(22), 12,125–12,134.
- Santolík, O., and Gurnett, D. A. (2003), Transverse dimensions of chorus in the source region,
- 445 Geophys. Res. Lett., 30, 1031, doi:10.1029/2002GL016178, 2.
- Santolik, O., Gurnett, D. A., & Pickett, J. S. (2004). Multipoint investigation of the source region
- of storm-time chorus. In Annales Geophysicae (Vol. 22, pp. 2555–2563).
- Shen, X. C., Hudson, M. K., Jaynes, A. N., Shi, Q., Tian, A., Claudepierre, S. G., ... Sun, W. J.

- 449 (2017). Statistical study of the storm time radiation belt evolution during Van Allen Probes era:
- 450 CME- versus CIR-driven storms. Journal of Geophysical Research: Space Physics, 122(8),
- 451 8327–8339.
- 452 Silva, C. L., Denton, R. E., Hudson, M. K., Millan, R. M., Liu, K., & Bortnik, J. (2018). Test-
- particle simulations of linear and nonlinear interactions between a 2-D whistler-mode wave
- packet and radiation belt electrons. Geophysical Research Letters, 45, 5234–5245.
- 455 https://doi.org/10.1029/2018GL077877
- Summers, D., Ni, B., & Meredith, N. P. (2007). Timescales for radiation belt electron
- acceleration and loss due to resonant wave-particle interactions: 2. Evaluation for VLF chorus,
- ELF hiss, and electromagnetic ion cyclotron waves. Journal of Geophysical Research: Space
- 459 Physics, 112(A), A04207.
- Tao, X., J. Bortnik, J. M. Albert, R. M. Thorne, and W. Li (2014), Effects of discreteness of
- chorus waves on quasilinear diffusion-based modeling of energetic electron dynamics, J.
- 462 Geophys. Res. Space Physics, 119, 8848–8857, doi:10.1002/2014JA020022.
- Thorne, R. M., Ni, B., Tao, X., Horne, R. B., & Meredith, N. P. (2010). Scattering by chorus
- waves as the dominant cause of diffuse auroral precipitation. Nature, 467(7318), 943–946.
- Thorne, R. M. et al. (2013), Rapid local acceleration of relativistic radiation belt electrons by
- magnetospheric chorus, Nature, 504, 411-414, doi:10.1038/nature12889.
- Tu, W., G. S. Cunningham, Y. Chen, S. K. Morley, G. D. Reeves, J. B. Blake, D. N. Baker,
- and H. Spence (2014), Event-specific chorus wave and electron seed population models in
- DREAM3D using the Van Allen Probes, Geophys. Res. Lett., 41, doi:10.1002/2013GL058819.
- Turner, D. L., Kilpua, E. K. J., Hietala, H., Claudepierre, S. G., O'Brien, T. P., Fennell, J. F., et
- al. (2019). The response of Earth's electron radiation belts to geomagnetic storms: Statistics from
- 472 the Van Allen Probes era including effects from different storm drivers. Journal of Geophysical
- 473 Research: Space Physics, 124. https://doi.org/10.1029/2018JA026066
- 474 Xiao, F., et al. (2014), Chorus acceleration of radiation belt relativistic electrons during March
- 2013 geomagnetic storm, J. Geophys. Res. Space Physics, 119, 3325–3332,
- 476 doi:10.1002/2014JA019822.

482

483

484

485

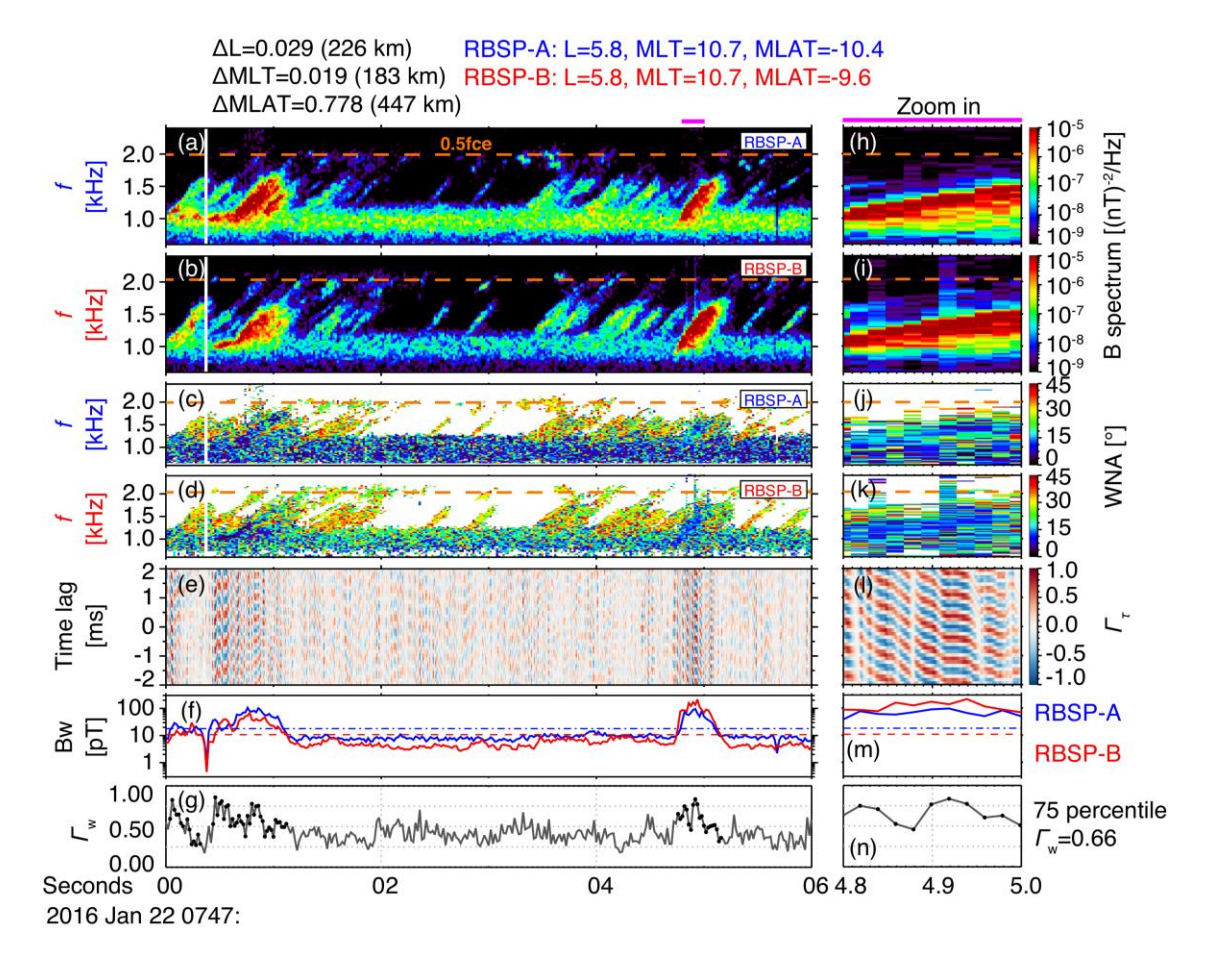
486

487

488

489

490



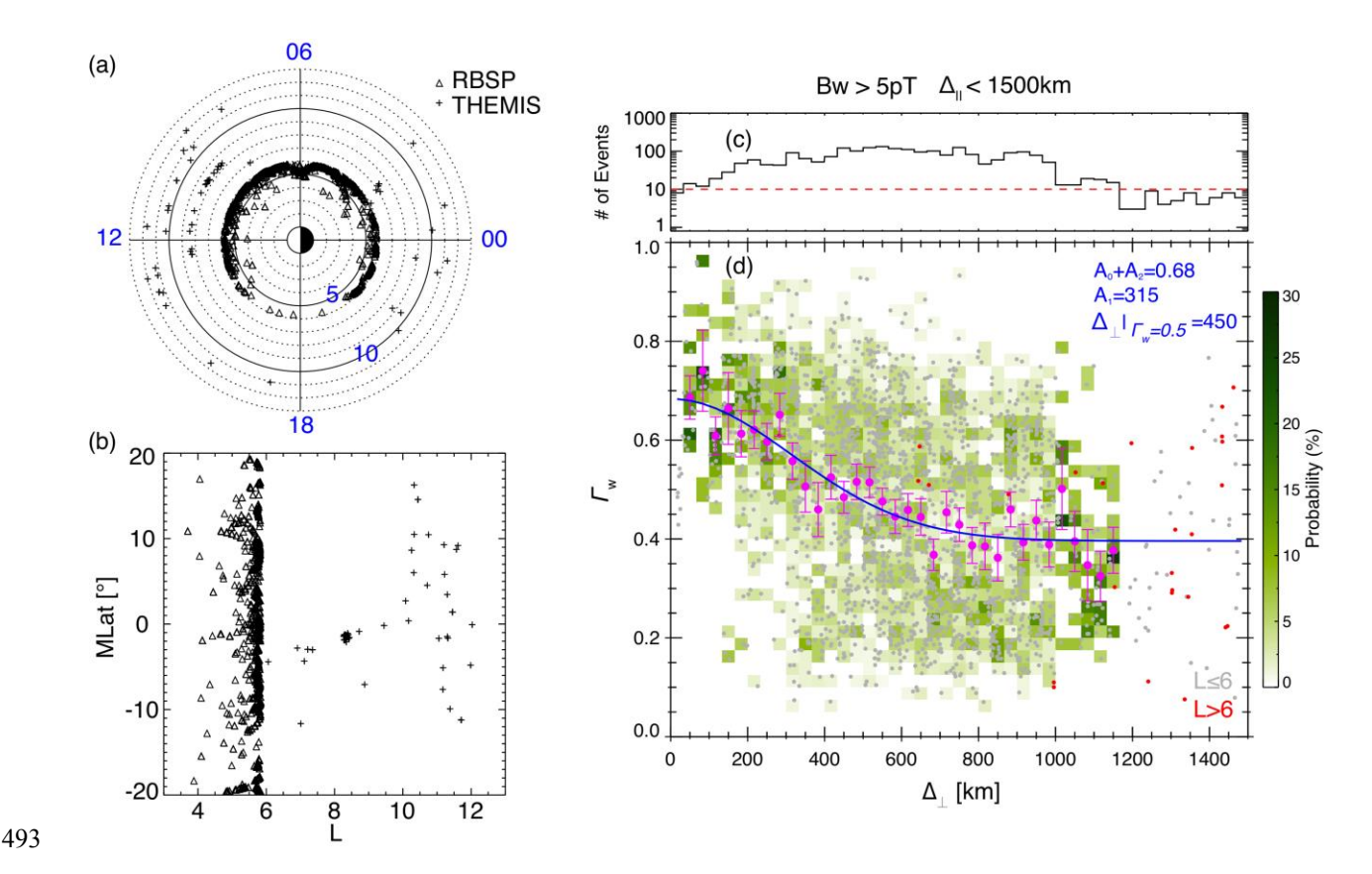


Figure 2. Event distribution and overall result of calculated correlation coefficients. (a) Event distribution in *L*-MLT and (b) *L*-MLAT planes. Events observed by a pair of RBSP (THEMIS) are marked as triangles (crosses). (c) Number of samples as a function of transverse separation distance. (d) Correlation coefficient as a function of transverse separation distance. Grey (red) dots are calculated correlation coefficients at L < 6 (L > 6). Greenish bins are probabilities of correlation coefficients in each $\Delta_{\perp} \times \Gamma_{\rm w}$ bin. Magenta dots are averaged correlation coefficients in each Δ_{\perp} bin with error bars indicating the standard error (σ). Blue line is the Gaussian fitting for the magenta dots and the corresponding fitting parameters are labeled in the right-top corner in panel (d).

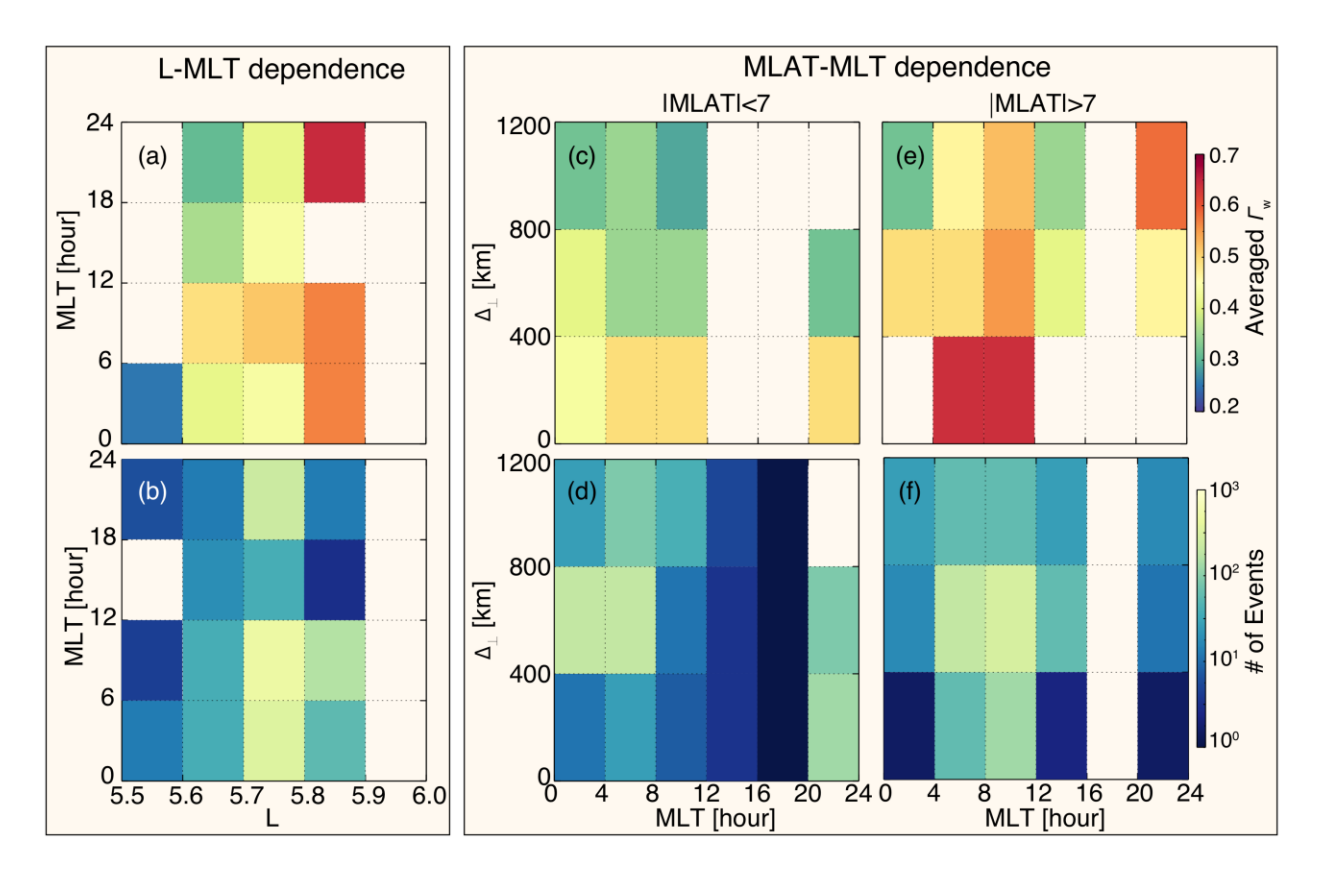


Figure 3. Dependencies of correlation coefficients of chorus waveform on L shell, MLT and MLAT. (a) Averaged correlation coefficient and (b) number of events in each $L \times \text{MLT}$ bin. (c) Averaged correlation coefficient and (d) number of events in each MLT $\times \Delta_{\perp}$ bin with |MLAT| < 7° in both northern and southern hemispheres. (e)-(f) are in the same format as (c)-(d), but for |MLAT| > 7°. For top panels, bins with fewer than ten event samples are not shown.

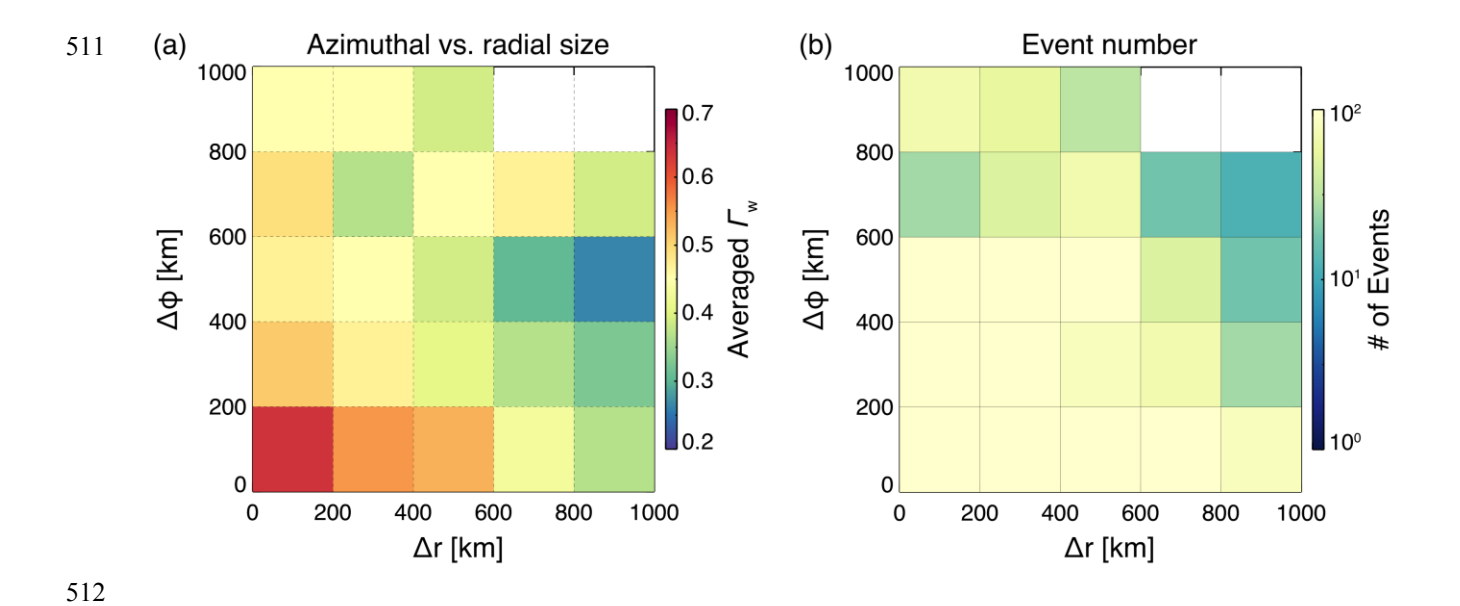


Figure 4. Azimuthal versus radial scale size of chorus waves. (a) Averaged correlation coefficient and (b) number of events in each $\Delta r \times \Delta \varphi$ bin, where Δr is the radial separation and $\Delta \varphi$ is the azimuthal separation of a pair of satellites.

514

